OH radicals distribution in an Ar-H2O atmospheric plasma jet

L. Li, A. Nikiforov, Q. Xiong, N. Britun, R. Snyders et al.

Additional information on Phys. Plasmas

OH radicals distribution in an Ar-H₂O atmospheric plasma jet

L. Li,[1] A. Nikiforov,[1,2,a)] Q. Xiong,[1,3] N. Britun,[4] R. Snyders,[4,5] X. Lu,[3] and C. Leys[1]

[1]*Department of Applied Physics, Research Unit Plasma Technology, Ghent University, Sint-Pietersnieuwstraat 41, Ghent B-9000, Belgium*
[2]*Institute of Solution Chemistry of the Russian Academy of Sciences, Academicheskaya St., 1, Ivanono, 153045, Russia*
[3]*College of Electrical and Electronic Engineering, HuaZhong University of Science and Technology, WuHan, Hubei 430074, China*
[4]*Chimie des Interactions Plasma-Surface (ChIPS), CIRMAP, Universite de Mons, 20 Place du Parc, B-7000 Mons, Belgium*
[5]*Materia Nova Research Centre, Parc Initialis, B-7000 Mons, Belgium*

Recently, plasma jet systems found numerous applications in the field of biomedicine and treatment of temperature-sensitive materials. OH radicals are one of the main active species produced by these plasmas. Present study deals with the investigation of RF atmospheric pressure plasma jet in terms of OH radicals production by admixture of H₂O into argon used as a feed gas. Generation of OH radicals is studied by laser-induced fluorescence spectroscopy. The excitation dynamics of OH radicals induced by the laser photons is studied by time-resolved spectroscopy. It is shown that vibrational and rotational energy transfer processes, which are sensitive to the surrounding species, can lead to the complication in the OH radicals diagnostics at high pressure and have to be considered during experiments. The axial and radial 2D maps of absolute densities of hydroxyl radicals at different water contents are obtained. The highest density of $1.15 \times 10^{20} \, \mathrm{m}^{-3}$ is measured in the plasma core for the case of 0.3% H₂O. In the x–y-plane, the OH density steeply decreases within a range of $\pm 2 \, \mathrm{mm}$ from its maximum value down to $10^{18} \, \mathrm{m}^{-3}$. The effect of H₂O addition on the generation of OH radicals is investigated and discussed. © *2013 AIP Publishing LLC*. [http://dx.doi.org/10.1063/1.4820945]

I. INTRODUCTION

Atmospheric pressure plasma jets (APPJs) are characterized by high concentration of radicals and low gas temperature. There is a growing interest in a view of considerable environmental, bio-medical, and material processing demands.[1–3] In the listed applications, radicals play a significant role and the plasma jet is often operated in the humid atmosphere. Therefore, the hydroxyl radical (OH), one of the strongest oxidative species generated in the water containing plasma, is assumed to be a key reactive agent in the plasma jets application. In a water-containing plasma jet, plasma operation conditions as well as the formation of hydroxyl radicals are determined by the relative humidity in the plasma. Moreover, in biomedical applications, plasma is commonly used to treat samples in solutions, where gaseous phase may contain a high amount of water. The study of the water addition effect to such plasma can give an insight on the possible mechanism of the OH radicals formation. The influence of water admixture on the plasma conditions has already been studied in the past.[4–6] Most of these studies, however, are limited by the optical emission spectroscopy which gives information about excited particles only. Optical emission spectroscopy concerns only the excited species which have quite low concentrations compared to their ground states. Because of this, the conclusions on the atomic

ground states density require rather complex models, which often are not available.

In this study, the effect of water vapor addition (varying from 0% to 1%) on OH generation is investigated in the H₂O-Ar admixture atmospheric RF plasma jet by spatially resolved laser-induced fluorescence (LIF) of OH radicals. LIF is an advanced laser-based plasma diagnostics technique enabling a direct access to the relative ground state densities of the probed species.[7] The potential of this technique has been demonstrated in the numerous works for characterization of the population densities and velocity distributions (temperatures) of atoms, molecules, and ions in several atmospheric plasma sources.[8,9]

Quantitative detection of the species of interest by LIF technique involves a proper interpretation of the obtained experimental results. Of particular complexity are the depopulation processes of the laser-excited states, including collisional quenching, rotational (RET) and vibrational (VET) energy transfer, and spontaneous emission from the excited state. In this paper, the influence of the water concentration and other surrounding species (diffused air and the plasma forming gas) on the kinetics of the laser excited OH radicals is investigated. In addition, a model taking into account both RET and VET processes is implemented in order to calculate the absolute density and 2D map distribution of OH radicals. It has to be noted that, the absolute density of OH radicals in plasma jets has already been detected by LIF[10] and cavity ring-down spectroscopy.[11] However, not enough attention has been paid to the influence of water

---

a)Electronic mail: anton.nikiforov@ugent.be

content on spatial distribution of OH radicals in the studied plasmas, as well as on the fluorescence generation processes after laser excitation of OH radicals. The last two aspects are the main subject of the present work.

II. THE EXPERIMENT AND DIAGNOSTIC METHODS

A schematic diagram of the system used in this work is presented in Fig. 1. The typical experimental parameters are listed in Table I. The capacitive-coupled plasma (CCP) jet with L-matching impedance box was sustained in open air. The RF electrode was made of tungsten pin of 1 mm diameter centered inside of a quartz capillary of 2 mm inner diameter. Grounded electrode had a ring shape and is placed around the capillary. Ar gas flow was equal to 2 slm (standard liter per minute) and was used as a feeding gas. Pure argon was fed into the plasma jet through two separated lines. One of the two connected lines went through a water bubbler filled with distilled water. The water vapor concentration in the discharge was determined assuming that the argon flow which passed through the water bubbler was saturated with water vapor at the room temperature. The water bubbler was calibrated in independent experiments up to flow of 4 slm with MiniRAE^{3000} gas phase analyzer equipped with H_2O detection tube. Calibration has shown that gas phase is saturated with water vapor in our experimental conditions. The amount of water added to the plasma jet can be varied from 0% to 1%. The plasma power was fixed at 10 W through all

experiments. The required gas temperature (T_{gas}) for interpretation of experimental data was estimated by means of optical emission spectroscopy. In order to evaluate T_{gas}, the high resolution spectrum (resolution of 0.05 nm) of the OH(A–X) v''-v' = 0-0 emission band in the spectral interval between 306 and 311 nm was measured by means of the Avantes 3648 spectrometer. The details of the techniques used for T_g determination by the OH(A–X) v''-v'' = 0-0 emission and their drawbacks can be found elsewhere.[6,12]

As shown in Fig. 1, the Sirah Cobra-Stretch dye laser (Rhodamine 590 as the dye) equipped with second harmonic generation unit and pumped by a pulsed Nd:YAG laser was utilized to excite the ground-state OH radicals $X^2\Pi$, v'' = 0 to the $A^2\sum^+$, v' = 1 by three excitation transitions, namely, $P_2(6)$, $P_1(4)$, and $P_2(3)$, all at around 283 nm. The laser pulse has a repetition frequency of 10 Hz and the pulse duration of about 5 ns. The laser energy per pulse was kept in the range of 10–20 μJ providing the LIF signal being always linearly proportional to the laser energy (so called "linear mode"). The energy was real-time monitored by a laser energy measurement head (Ophir PE-9). The laser beam after beam shaping optics had rectangular shape with the cross-section area in the vicinity of the discharge of about 7×0.5 mm^2, as shown in Fig. 1(b)). The OH fluorescence signal was collected at about 15 cm away from the jet location by an Andor iStar 740 ICCD camera perpendicularly to the laser beam direction through the optical band pass filter with a central wavelength of 309 nm and full width in half maximum
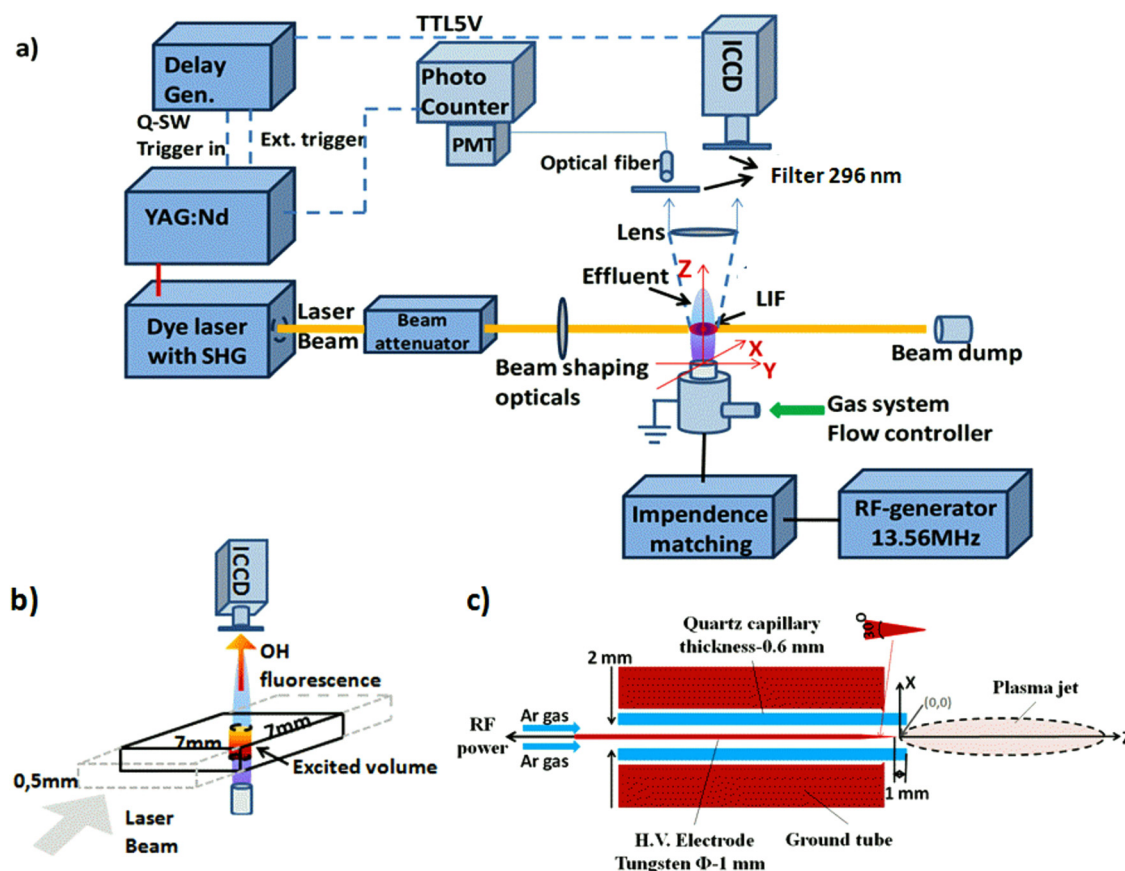

FIG. 1. (a) Schematic of the experimental set-up used for the measurement of OH radicals in the atmospheric pressure RF plasma jet; (b) Beam path for the LIF measurements; (c) The drawing of the plasma jet device.

TABLE I. The experimental parameters used in this work.

| Experimental parameter	Value/Description
Discharge RF frequency	13.56 MHz
Averaged RF power	10 W
Used gas, flow rate	Ar + H$_2$O, 2 slm
Pumping laser	Spectra Physics INDI YAG:Nd on 532 nm
Dye laser	Sirah Cobra Stretch with SHG unit
Used dye, wavelength	Rhodamine 590, 284 nm
Laser energy per pulse	10–20 μJ
Laser spectral linewidth	0.03 cm^{-1}
Laser frequency	10 Hz
Laser pulse duration (FWHM)	∼5 ns
ICCD camera	AndoriStar740
Spectrometer, entrance slit size	Andor Shamrock 750, 50 μm
Gate time (utilized in the time-resolved measurements)	20 ns (LIF spectroscopy), 5 ns (LIF imaging)

(FWHM) of about 10 nm. The ICCD camera was also used to record the spatially resolved discharge cross sections in terms of OH density. The time-jitter of the whole setup was estimated to be about 1 ns. The wavelength-resolved fluorescence signal of the OH ro-vibrational bands (308 nm, with 0.03 nm resolution) was detected in the same system by sending the fluorescence signal through an Andor Shamrock 750 spectrometer. Calibration of the LIF signal was carried out by the commonly used Rayleigh scattering technique at the wavelength 309 nm,[15] i.e., close to maximum transparency of the used optical filter based on 2D images of the Rayleigh scattering of the laser beam.

## III. RESULTS AND DISCUSSION

The appearance of the studied plasma jet afterglow at different water concentrations is illustrated in Fig. 2. Its length is strongly affected by water content and decreases from 13 mm in pure Ar to less than 6 mm at 1% H$_2$O. In the meantime, the emission spectra of the discharge consist mainly of the OH emission bands, as well as the Ar peaks. Relatively weak emissions from the nitrogen second positive system N$_2$(C-B) (with a band head at 337 nm), as well as from H$_\alpha$ line at 656 nm and H$_\beta$ line at 486 nm is also observed. Moreover, the N$_2$ emission remains detectable even inside the jet nozzle at low water contents due to the air diffusion into the nozzle. An increase of the water content leads to a fast decrease of the N$_2$(C-B) emission in the whole afterglow of the jet which is different from the effect of H$_2$O addition on the OH(A) emission. The decrease of the N$_2$(C-B) emission can be correlated with probable decrease in the electron temperature at high water contents. On the other hand, the emission of OH(A) depends non-linearly on the water content with local minimum at 0.18% H$_2$O. Since the recorded emission from this state depends on several production and quenching processes, primarily determined by the following reactions:[13] Dissociative electron excitation of water
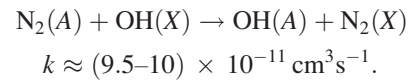
$$\text{H}_2\text{O} + \bar{e} \rightarrow \text{OH}(A) + \text{H} + e \qquad k \approx 10^{-11}\,\text{cm}^3\text{s}^{-1}$$
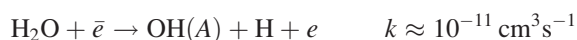
Dissociation recombination of water ions

$$\text{H}_2\text{O}^+(\text{H}_3\text{O}^+) + \bar{e} \rightarrow \text{OH}(A) + \text{H} \quad k \approx 10^{-8} - 10^{-10}\,\text{cm}^3\text{s}^{-1},$$
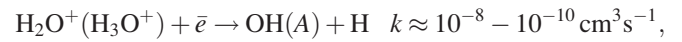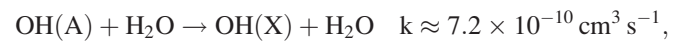
where ions are formed by Penning ionization with Ar^m or by the electrons impact. Direct electrons excitation of the ground state OH(X):

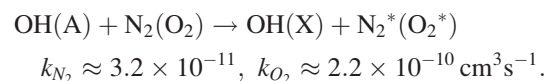$$\text{OH(X)} + \bar{e} \rightarrow \text{OH}(A) \quad k \approx 2.7 \times 10^{-10}\,\text{cm}^3\text{s}^{-1}.$$
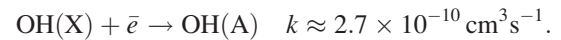
The pooling reaction of OH(A) excitation by N$_2$(A)[14]

$$\text{N}_2(A) + \text{OH}(X) \rightarrow \text{OH}(A) + \text{N}_2(X)$$
$$k \approx (9.5\text{–}10) \times 10^{-11}\,\text{cm}^3\text{s}^{-1}.$$

The main loss mechanism of OH(A) at high water content is determined by quenching with H$_2$O (Ref. 10)

$$\text{OH}(A) + \text{H}_2\text{O} \rightarrow \text{OH(X)} + \text{H}_2\text{O} \quad k \approx 7.2 \times 10^{-10}\,\text{cm}^3\,\text{s}^{-1},$$

while at low water contents the quenching of OH(A) by N$_2$ and O$_2$ (appearing in the discharge zone due to back-diffusion of air) plays an important role[18]

$$\text{OH}(A) + \text{N}_2(\text{O}_2) \rightarrow \text{OH(X)} + \text{N}_2^*(\text{O}_2^*)$$
$$k_{N_2} \approx 3.2 \times 10^{-11}, \ k_{O_2} \approx 2.2 \times 10^{-10}\,\text{cm}^3\text{s}^{-1}.$$

Unfortunately, the optical emission spectroscopy cannot provide direct relations between the intensity of the OH(A)-related emission bands and the OH radicals ground density. In order to obtain the distribution of the ground state OH radicals in the afterglow, and to investigate the influence of the water content on this distribution, the LIF technique has been used. It should be noted, however, that one of the drawbacks of the LIF technique is that the collisions between the surrounding heavy particles and the laser-excited radicals may alter the experimentally registered LIF signal and so the further interpretation of the results. This is a crucial point for the rigorous interpretation of the LIF results in the atmospheric pressure plasmas with high frequency of collisions when the colliding particles such as H$_2$O, N$_2$, and O$_2$ (due to air back diffusion into the jet) have to be considered. The
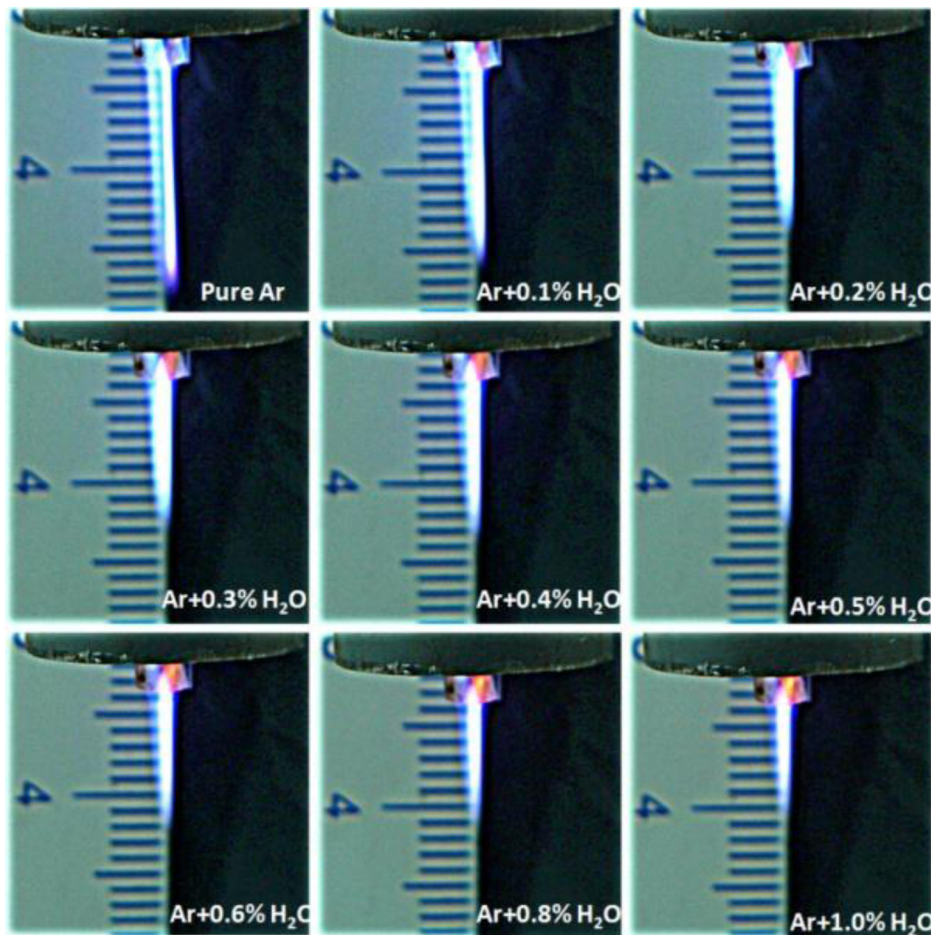
FIG. 2. Images of RF plasma jet in Ar/ H_2O mixture. The Ar flow rate is 2 slm, water concentration is ranged from 0% to 1%.

detailed description of the performed LIF measurements of the OH radicals in the discharge, the obtained LIF results, as well as their analysis and discussion are presented in the following subsections.

A. Temporal behavior of the laser-excited OH states: Collisional energy transfer

The scheme of the LIF processes along with the typical LIF spectra and rotational distribution of OH radicals after excitation of $P_1(4)$ branch at 20 ns time after the laser pulse (Δt) are shown in Fig. 3. The value Δt is referred to the time delay after the beginning of the laser pulse. The transitions $P_1(4)$, $P_2(3)$, $P_2(6)$ of the $X^2\Pi$ state of OH radicals were laser-excited to the vibrational level $v' = 1$ of $A^2\Sigma^+$ state (see Fig. 3). After the laser pulse, a strong emission in the spectral range of 312–316 nm appears in the LIF spectra which belongs to the radiative transition between level $v' = 1$ of $A^2\Sigma^+$ and $X^2\Pi$ $v'' = 1$. An overpopulation of the vibrational level $v' = 1$ is observed, having the relative population of 0.56 at $\Delta t = 20$ ns due to the laser pumping. It has to be noted that the population of the level $A^2\Sigma^+$, $v' = 0$ seems to be essential even at $\Delta t = 20$ ns with the population degree of 0.44. The strong radiative emission from the level $A^2\Sigma^+$, $v' = 0$ at $\Delta t = 20$ ns can be attributed to the fast VET process. Furthermore, at $\Delta t = 20$–40 ns, the intensity of the band v''-$v' = 1$-1 drastically decreases, whereas much stronger band v''-$v' = 0$-0 starts to dominate in all the spectra. The observed decrease of v''-$v' = 1$-1 band emission is mainly due to the

VET in between level $v' = 1$ and $v' = 0$ of $A^2\Sigma^+$ due to collisions with Ar and H_2O. The cross-sections of VET processes for $A^2\Sigma^+$ ($v' = 1$ to $v' = 0$) with H_2O (Ref. 16) is about 8.6 ± 0.6 Å^2 corresponding to the rate coefficient of 4.04×10^{-11} cm^3 s^{-1} ($T_g = 500$ K). The quenching cross sections has been converted to the rate coefficients by the relationship

$$k = \sigma v, \qquad (1)$$

where the average collision velocity is

$$\langle v \rangle = (8kT_g/\pi\mu)^{1/2}. \qquad (2)$$

Here, k is the Boltzmann constant, T_g is the gas temperature, and μ is the reduced mass of the collision pair. The small density of water as a collider in our experiments results to characteristic time of VET process $\tau^{VET} = 5.8$ μs due to collisions with H_2O only. This value is longer than the experimentally observed time of 20 ns and the discrepancy can be explained by VET induced through collisions with Ar. VET cross-section of the OH radicals with Ar is 0.44 ± 0.06 Å^2 (Ref. 16) corresponding to the rate coefficient 1.68×10^{-12} cm^3 s^{-1} ($T_g = 500$ K), resulting in shorter τ^{VET} of 15–25 ns. Correspondingly, after the OH radicals are excited by the laser, the VET transfer is determined mainly by collisions with Ar rather than with H_2O.

Due to rather the narrow laser beam (0.5×7 mm^2) which was utilized in this study for OH excitation, the space resolved OH distribution at the effluent of the jet can be

investigated. The time-resolved LIF signal cross-sections of the jet give an insight into the spatial profile of the OH radicals in the discharge and dynamics of the OH radicals excitation. Typical time-resolved images of OH fluorescence presented in Fig. 4(a) are corrected by subtracting the plasma emission. Meantime, Fig. 4(b) represents the time-decay of the wavelength-integrated LIF signal obtained at the distance equal to 1 mm away from the nozzle. The presented time decay corresponds to the integration of the LIF signal over the central zone of the discharge with a diameter of 1 mm. Dynamics of OH fluorescence after the laser pumping is characterized by a gradual exponential decay for the entire cross section with the decay time equal to 59 ns. On the other hand, the decay time corresponding to radiative depopulation of OH $A^2\Sigma^+$ to ground state is reported to be about 0.685×10^{-6} s.[17] Thus, the observed much shorter value is likely determined by the collisional quenching of OH with H_2O, whereas the quenching by Ar is much weaker. Paul[18] postulated that quenching occurs via an ion-pair intermediate

$$OH(A^2\Sigma^+) + H_2O \rightarrow OH^-(X^1\Sigma^+)$$
$$+ H_2O^+ \rightarrow OH(X^2\Pi_i) + H_2O.$$
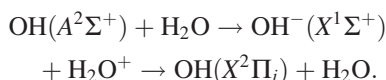
With the decay time determined as

$$\tau^{-1} = A_f + k_Q[H_2O], \qquad (3)$$

where A_f is Einstein coefficient of spontaneous emission and k_Q is a quenching rate constant. Nevertheless, quenching of OH by H_2O with the rate constant of 68×10^{-11} cm^3 s^{-1} (Ref. 22) at 0.3% H_2O results in the decay time equals to 70–100 ns which is slightly longer than experimental measured value presented in Fig. 4(b). We suggest that the observed decay time of 59 ns (the case of 0.3% H_2O at $z = 1$ mm) can be associated with additional quenching of OH(A) by N_2 and O_2 appearing in the plasma zone due to the air diffusion in the jet that provides a way to calculate the air molar fraction in the discharge.

Furthermore, at the beginning, up to the time $\Delta t = 20$ ns, when emission from the band OH(X-A) v''-$v' = 1$-1 is still strong, the radial distribution of LIF intensity in the core of the discharge is very uniform. Later on at $\Delta t = 45$–180 ns, it has almost Gaussian distribution along the jet radius. Consequently, the obtained LIF images taking at different time after the laser pulse may not correspond to the real OH ground state density distribution, being substantially affected by VET and collisional quenching process. As a result, the measured OH distribution will strongly depend on the time of images acquisition. For the accurate quantification of the radicals density in the RF jet, it is necessary to analyze the dynamics of the laser excited OH radicals. To address this issue, the high resolution LIF v''-$v' = 0$-0 band rotational spectra of OH ($A^2\sum^+$-$X^2\Pi$) (307–312 nm) was measured as
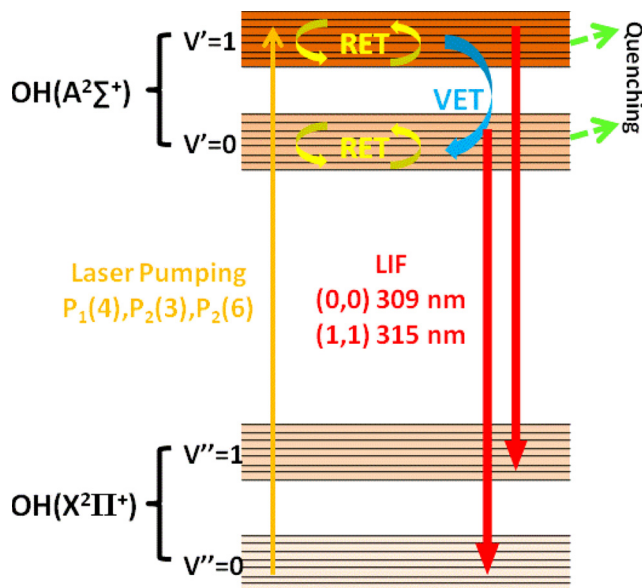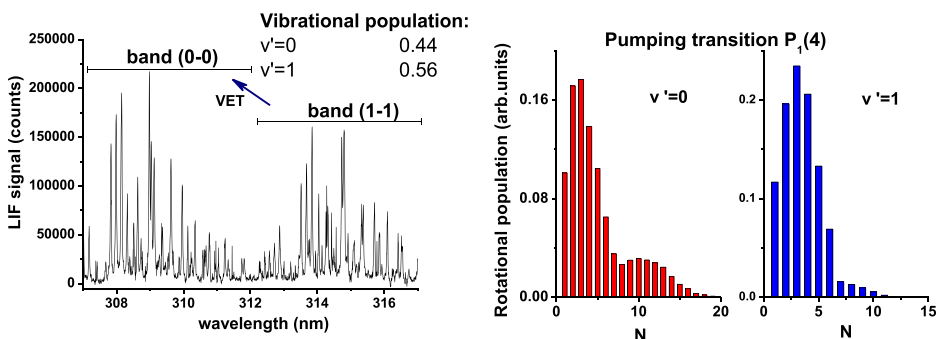

FIG. 3. Scheme of laser excitation processes of the LIF spectra generation and typical LIF spectra of OH radicals at $\Delta t = 20$ ns (exposition time 20 ns, excited transition $P_1(4)$).
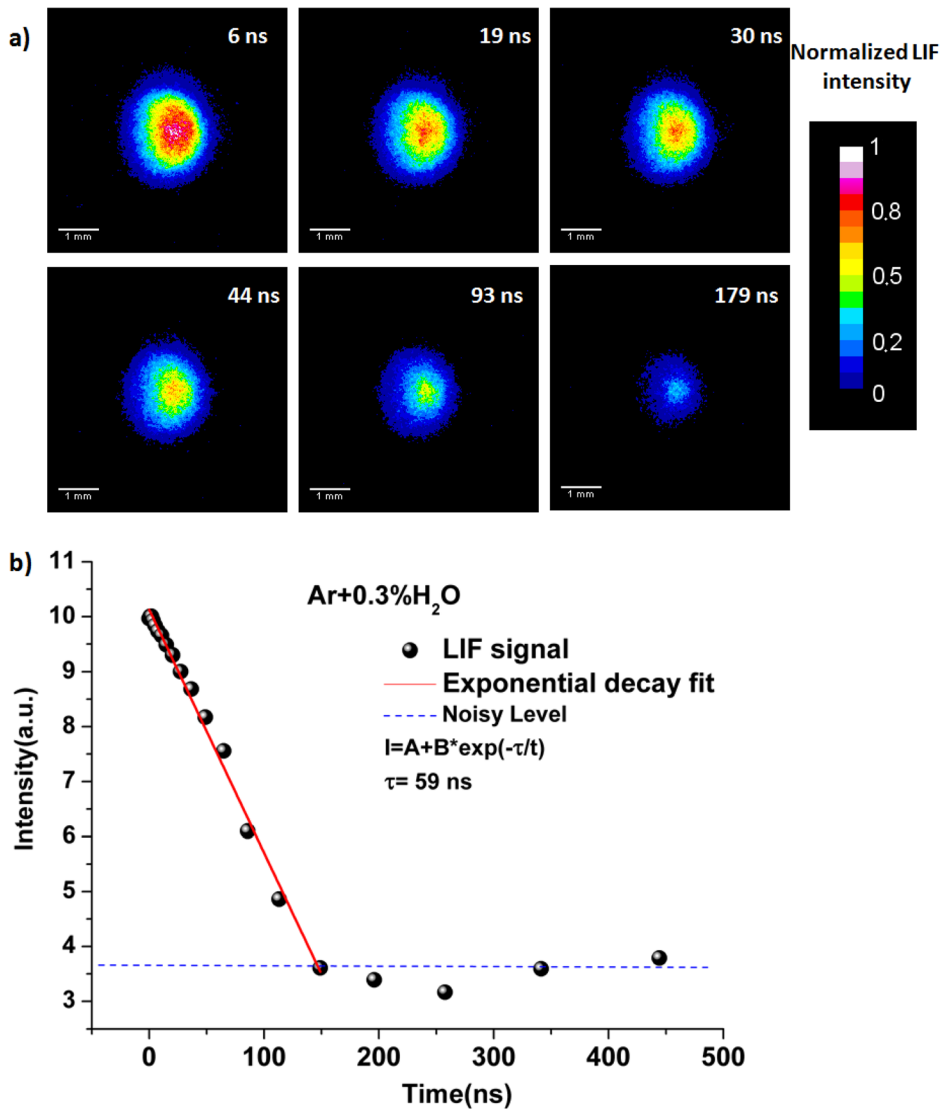
FIG. 4. Temporal variation of OH radicals LIF signal of the jet effluent excited on $P_2(3)$ transition. (a) Time resolved LIF signal of the effluent at different Δt. (b) Time decay of spectrally integrated LIF signal from bands $v''\text{-}v' = 0\text{-}0$ and $v''\text{-}v' = 1\text{-}1$. LIF signal is corrected by subtraction of plasma emission. Noise on (b) is mostly due to dark current of the ICCD.

function of Δt. Figure 5 represents laser excited spectrum of OH at $\Delta t = 20$ ns, 60 ns, and 120 ns, respectively, along with the corresponding rotational distribution of OH radicals of $A^2\textstyle\sum^+$, $v' = 0$. The rotational distribution is compared to the Boltzmann distribution at 500 K where the temperature of 500 ± 50 K in RF plasma jet is estimated by optical emission spectroscopy of OH $(A^2\textstyle\sum^+\text{-}X^2\Pi)$ $v''\text{-}v' = 0\text{-}0$ band. It is obvious that at $\Delta t = 20$ ns, the rotational population distribution of laser excited OH radicals is non-Boltzmann. Only the rotational states with the low rotational numbers ($J \leq 3$) are in thermal equilibrium. Instead, an overpopulation of higher rotational states ($J > 7$) appears. Moreover, the population of rotational levels corresponding to the rotational numbers higher than $J = 12$ is characterized by Boltzmann distribution with significantly higher temperature (about 1500 K). Nevertheless, 40–60 ns later, the overpopulation at high rotational states disappears probably due to fast RET processes and slight overpopulation at J < 3 is observed. The OH rotational population starts to be thermal with temperature of about 500 K only at $\Delta t \approx 120$ ns. The observed Boltzmann distribution close to 500 K at $J < 3$ even at $\Delta t = 20\text{–}50$ ns is probably explained by the fact that the RET transfer is faster for low rotational levels. Overpopulation of the higher

rotational states may be attributed to the $A^2\textstyle\sum^+$, $v' = 0$ populating process involving the VET process and collisions with Ar, as it described in Refs. 16 and 19. The present results show that VET and RET in the atmospheric pressure plasma jet can contribute to the complication in the scheme of OH ro-vibrational levels population during the laser pumping. Thus, both VET and RET have to be considered if wavelength-integrated LIF signal is used for the determination of the OH density.

B. Model of OH radicals laser excitation

Based on results presented in Sec. III A, it can be stated that the temporally integrated broadband fluorescence intensity is determined by the spontaneous emission as well as the collisional energy transfer processes such as quenching, predissociation, VET, and RET. Therefore, it is required to clarify the proportionality between the fluorescence intensity from the upper states and the concentration of the ground state OH radicals. The VET and RET in the upper state act to redistribute the population from the laser excited level to other ro-vibronic states. One of the well-known approaches for the LIF signal interpretation employed for direct absolute
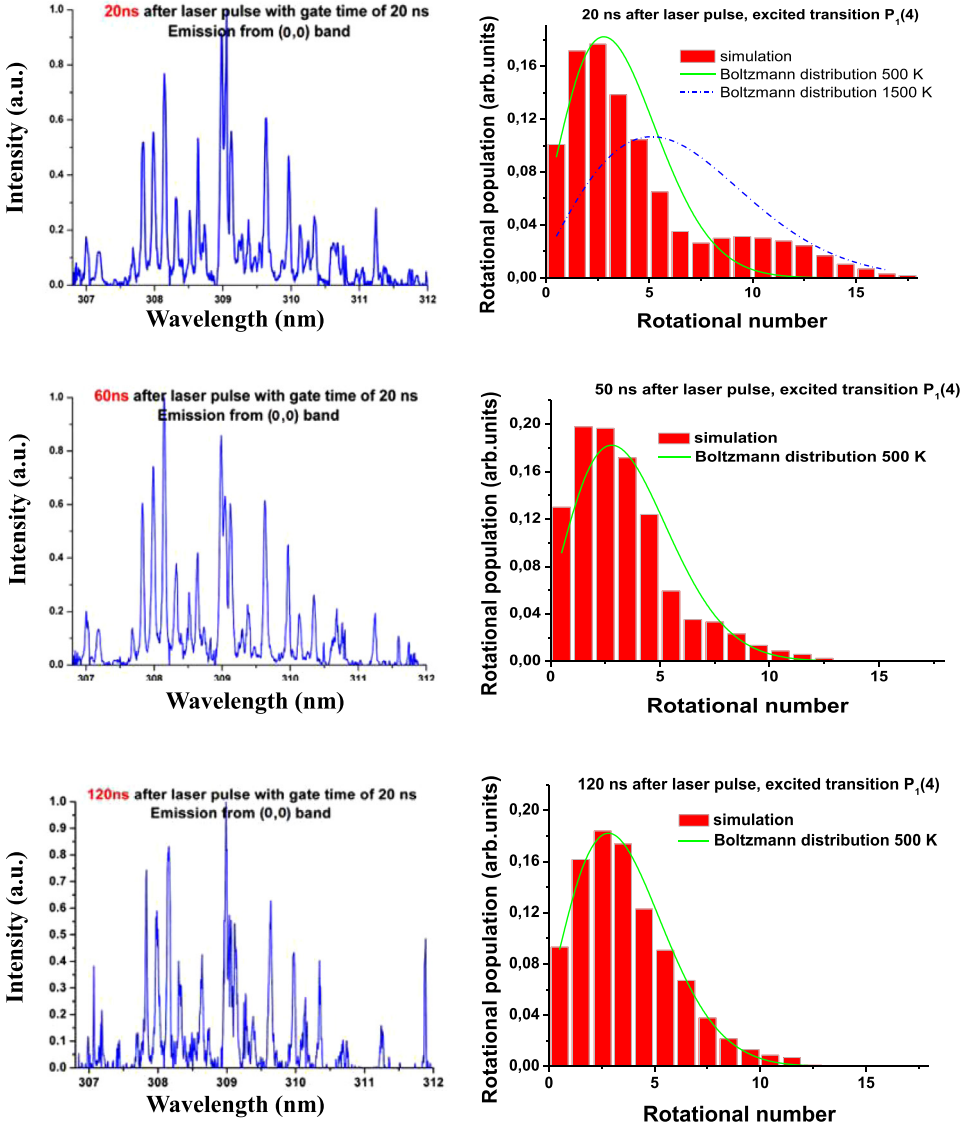
FIG. 5. The time-resolved LIF spectrum of OH v''-$v' = 0$-0 band (308 nm) at $\Delta t = 20\,\text{ns}$, 60 ns, and 120 ns, respectively. On the right, rotational populations of OH(A) ($A^2\sum^+$, $\nu' = 0$) at the corresponding time are presented.

radicals density calculations is so called "three level model."[5] It assumes that the molecules excited to the upper state remain in the original excited level until spontaneous emission.[5,10] Unfortunately, it is not valid for plasma jet at high pressure due to non-Boltzmann distribution in the upper energy levels deduced from the time-resolved LIF spectrum of OH $A^2\sum^+$ state. In the present work, we consider that the ground-state OH radicals $X^2\Pi$, $v'' = 0$ is excited to the $A^2\sum^+$, $v' = 1$ by the laser with the fluorescence appearing from v''-$v' = 0$-0 and v''-$v' = 1$-1 bands. The time-dependent population of the relevant energy levels can be expressed as follow:the laser-coupled upper rotational level i in $A^2\sum^+$,$v' = 1$

$$\frac{dn_i}{dt} = B_{xi}I_L n_x(t) + \sum_{j \neq i} R_{ji} n_j(t)$$
$$- \left(\sum_{j \neq i} R_{ij} + B_{ix}I_L + V_{(1\to 0),i} + A_i + Q_i\right) n_i(t) \quad (4)$$

the upper state levels j in the $A^2\sum^+$, $v' = 1$ populated by RET($j \neq i$)

$$\frac{dn_j}{dt} = \sum_{j \neq i} R_{ij} n_i(t) - \left(\sum_{j \neq i} R_{ji} + V_{(1\to 0),j} + A_j + Q_j\right) n_j(t) \quad (5)$$

the upper state levels i in the lower vibrational level $A^2\sum^+$, $v' = 0$ populated by VET

$$\frac{dn_{(v'=0),i}}{dt} = \sum_j V_{(1\to 0),j} n_j(t)\delta_i + \sum_{i \neq j} R_{(v'=0),ji} n_{(v'=0),j}(t)$$
$$- \left(\sum_{i \neq j} R_{(v'=0),ij} + A_{(v'=0),i} + Q_{(v'=0),i}\right) n_i(t) \quad (6)$$

the laser-coupled ground level x

$$\frac{dn_x}{dt} = B_{ix}I_L n_i(t) - B_{xi}I_L N_{OH}(t) + Q_{RET}N_{OH'}(t), \quad (7)$$

where I_L is the laser intensity, B_{xi} and B_{ix} are the rates for absorption and the stimulated emission, n_i is a density of radicals on corresponding level, R_{ij} is the state to state rate for RET from rotational level i to level j inside one vibrational level, $V_{(1\to 0),i}$ is the rate for VET from level i in $A^2\sum^+$,

$v' = 1$ to $A^2\sum^+$, $v' = 0$, A_i is Einstein coefficient of emission, Q_i is the quenching rate, and δ_i describes how the population is spread on the rotational levels of the $A^2\sum^+$, $v' = 0$. N_{OH} (t) can be considered as a constant during the laser pulse due to fast RET with rate constant about $3.5 \times 10^{-9}\,s^{-1}$ or higher.[18,20] The same approximation has been used by others[5,8] and gives very good agreement with experiment. The spectrally and temporally integrated fluorescence can be written as

$$I_{LIF} = G\Omega_{LIF}V_{LIF}\sum_l\left(\sum_m\frac{A_{lm}\varepsilon_{lm}t_{lm}}{4\pi}\int_0^\infty n_l dt\right), \quad (8)$$

where G is the efficiency of the optical system, Ω_{LIF} and V_{LIF} are the detection solid angle and light emitting volume, ε_{lm} is the energy gap of the corresponding transition from rotational level l to level m, and t_{lm} is the filter transmittance for the OH emission wavelength. It is reasonable to use the summation of upper state population over all the levels j as following:

$$\sum_l(Q_l + A_l)\int_0^\infty n_l dt = N_{OH}B_{xl}\int_0^\infty I_L dt. \quad (9)$$

Thus, the calibrated LIF signal intensity $I_{LIF}{}^0$ can be expressed in the relationship to N_{OH} as

$$I_{LIF}^0 = \eta N_{OH}B_{xl}\int_0^\infty I_L dt \quad (10)$$

η is the fluorescence yield, which represents the ratio of the molecules depopulated to the ground level due to fluorescence to the total number of the laser excited molecules.

$$\eta = \frac{\sum_l\left(\sum_m A_{lm}\varepsilon_{lm}t_{lm}\right)}{\sum_l A_l + Q_l}. \quad (11)$$

The fluorescence yield can be obtained, e.g., based on the LIF spectrum simulation by LASKIN.[21] The absolute concentration can be calculated based on Boltzmann distribution function as

$$n = \frac{n_x\sum_i g_i\exp[-E_i/kT]}{g_x\exp[-E_x/kT]}, \quad (12)$$

where E_i and g_i are the energy and statistic weight of the rotational level i.

C. Spatially resolved LIF and absolute OH density

The described above model has been applied for the determination of the absolute density of OH radicals in the RF jet afterglow in the following scheme:

(i)   Measurement of spatially and time resolved LIF signal with ICCD camera;

(ii)   Axial resolved calculation of air molar fraction from the decay time of LIF signal;

(iii)   Simulation of LIF spectra and calculation of the fluorescence yield η, see Eq. (11);

(iv)   Reconstruction of space resolved cross-section of OH radicals density taking in to account VET/RET processes.

The unknown air molar fraction in the jet has been estimated based on the measured decay time of the LIF signal. The idea behind the method based on the fact that the total fluorescence decay time (τ) is determined mainly by collisions with heavy particles see Eqs. (6), (7), and (9). The decay time τ can be experimentally determined at known admixture of H_2O into the Ar. On the other hand, the decay time can also be calculated by LIF spectra simulation, e.g., in Ref. 21 with variable density of colliders as an input parameter. In the present study, we consider the colliders with known density are Ar and H_2O and colliders with variable concentration from 0% to 15%: N_2, O_2, H_2O with ratio of 78:20:1.5, respectively. The quenching cross-section for Ar 0.047 Å^2 (Ref. 22) ($k = 0.45 \times 10^{-12}$ cm^3 s^{-1}, $T_g = 500\,K$) is much smaller than one for H_2O of 80 Å^2, ($k = 68 \times 10^{-11}$ cm^3 s^{-1}) but still was considered in the calculations because of the ground density of Ar is high in the feed gas. The best fit between the measured and calculated parameter τ gives a desired value of air molar fraction. In the simulation, except the effect of Ar and H_2O on quenching, VET, and RET, the energy transfer and quenching of OH(A) induced by N_2 and O_2 are also considered. The quenching cross-section for N_2 is 3.2 Å^2 ($k = 3.16 \times 10^{-11}$ cm^3 s^{-1}, $T_g = 500\,K$)[27] and for O_2 17.8 Å^2 ($k = 17.2 \times 10^{-11}$ cm^3 s^{-1}, $T_g = 500\,K$),[22] respectively. The dependence of quenching rate on rotational number J of OH(A) is described by empirical law derived by Kienle[21,23]

$$Q(J) = Q_0\exp(-J(J+1)(A + T_gB), \quad (13)$$

where Q_0 is the quenching rate corresponding to the lowest rotation level and parameters A and B for different colliders can be found in Refs. 22 and 23 and references herein. The VET cross-section for O_2 is 3.9 Å^2 ($k = 3.78 \times 10^{-11}$ cm^3 s^{-1}, $T_g = 500\,K$) and for N_2 is 24.5 Å^2 ($k = 24.3 \times 10^{-11}$ cm^3 s^{-1}, $T_g = 500\,K$)[16] with linear dependence on the rotational numbers described as following:

$$V(J) = V_0(1 - CJ), \quad (14)$$

where V_0 is VET rate corresponding to the lowest rotation level and value of C is 0.0343 for N_2 and 0.052 for O_2.[21] Upward vibrational energy transfer is not considered in the present study because of low probability in comparison with the probability of downward process. The air molar fraction has been calculated along the plasma jet axis as a radial spatial averaged value. The reason for approach comes from the fact that the experimental measurement of decay time may have high uncertainness in the outer sheath of the discharge and very time consuming. Figure 6 represents typical result of the air molar fraction, calculated with measured decay time of the LIF signal, as a function of distance from the jet nozzle. The systematic error of the measurements is about
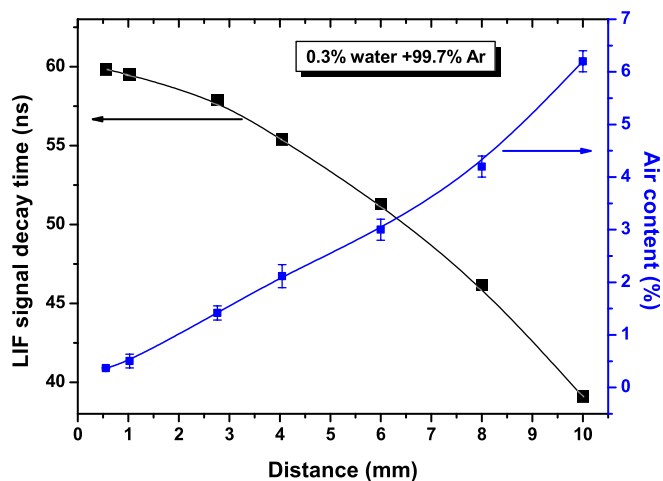
FIG. 6. Decay of LIF of OH radicals in the core of the RF jet and air content calculations at different distances from the nozzle.
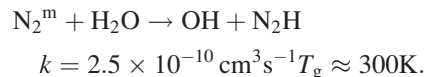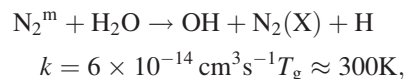
18% and it is mostly determined by the experimental error in measurement of the LIF signal. Though only the result for 0.3% H_2O is presented in Fig. 6, the results are similar for other mixtures. Based on the known molar fraction of air and LIF signal cross-sections, the absolute 2D density of OH radicals can thus be calculated in the afterglow. In Figure 7, the spatial distribution of the OH radicals is presented in the x–y-plane at z = 1, 3, and 8 mm for different water contents. It is found that the distribution of radicals is consistent with the jet geometric size. Correspondingly, generation of OH radicals takes place inside the plume region with highest OH density of $1.15 \times 10^{20}\,m^{-3}$ in the plasma core at the position $(x, y) = (0, 0)$ for the case of 0.3% H_2O. In the x–y-plane, the OH density steeply decreases within a range of $\pm 2\,mm$ from its maximum value down to $10^{18}\,m^{-3}$.

The radial cross-sections of the OH density from Fig. 7 can be recalculated into axial maps of OH radicals distribution in the afterglow of the RF jet. Figure 8 shows the spatial

distribution of OH radicals in the y–z-plane for different gas mixtures. Comparing the OH density distribution for different gas mixtures, it can be stated that not only the density of OH radicals but also the region where they are generated depends on the H_2O content. Indeed, at low water density, the OH density is still high ($1 \times 10^{19}\,m^{-3}$) on the distance of 13 mm away from the nozzle. The OH radicals are produced mainly in the place of mixing of feed gas with surrounding humid air. It is especially visible from the ring-shape of OH distribution in Fig. 7, cross-section at 3 mm distance with 0.1% H_2O. In our opinion, this ring shape is attributed to the generation of the radicals due to ion-neutral reactions and metastables-neutral reactions[24,25]

$$OH^+ + H_2O \rightarrow H_2O^+ + OH \quad k = 1.5 \times 10^{-9}\,cm^3\,s^{-1},$$

$$Ar^m + H_2O \rightarrow OH + H + Ar \quad k = 4.5 \times 10^{-10}\,cm^3\,s^{-1}.$$

The importance of the ion-neutral and metastable-neutral reactions in the OH radicals formation at low water content has also been confirmed by the simulation of Bruggeman.[13] The reactions mainly take place in the intensive mixing region of the feeding gas and diffused air, where H_2O density reaches maximum. Besides the suggested mechanisms, it appears possible that OH(X) can be produced, in the outer shell of the afterglow, through the reactions of water dissociation with N_2 metastables[26]

$$N_2{}^m + H_2O \rightarrow OH + N_2(X) + H$$
$$k = 6 \times 10^{-14}\,cm^3 s^{-1} T_g \approx 300K,$$

$$N_2{}^m + H_2O \rightarrow OH + N_2H$$
$$k = 2.5 \times 10^{-10}\,cm^3 s^{-1} T_g \approx 300K.$$

$N_2{}^m$ species are produced by non-resonance energy transfer in reactions of N_2 with Ar^m generated in the discharge core.
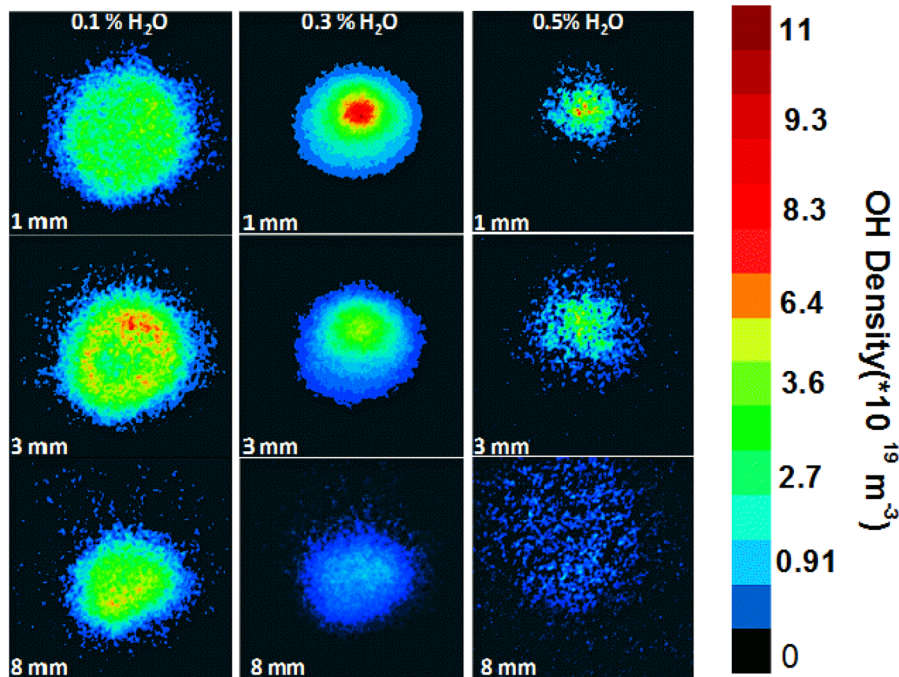

FIG. 7. Radial distribution of the OH density in the jet afterglow with variable admixture of water in different distances from the nozzle.
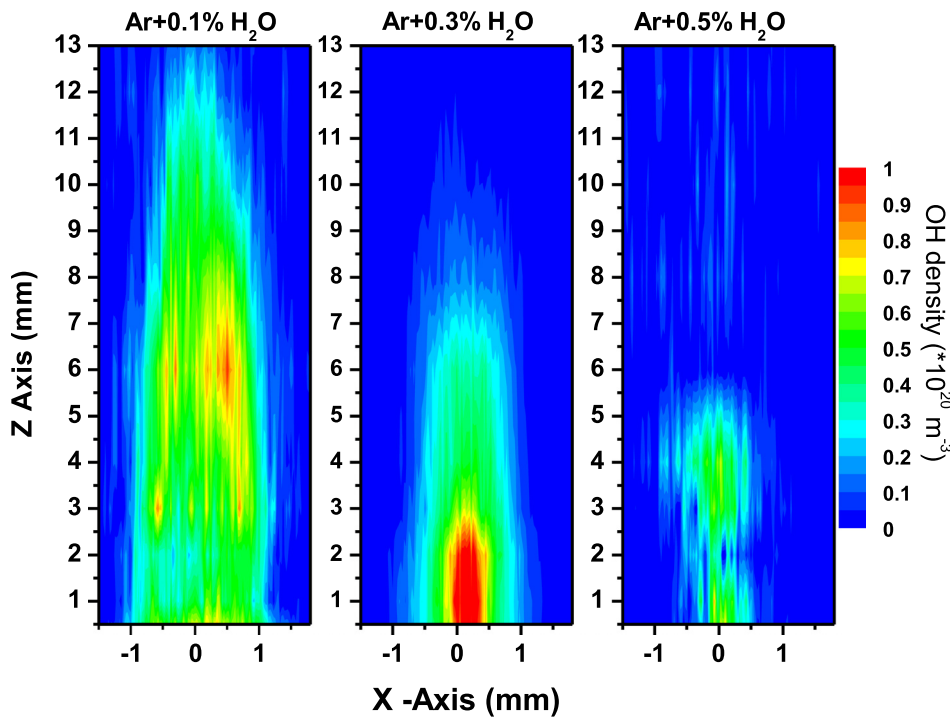
FIG. 8. Spatial distribution of the OH density in the jet afterglow.

The ring shape of OH distribution is detectable up to water content of 0.15% corresponding to 2.25×10^{20} m^{-3} of H$_2$O in the Ar gas at 500 K. Conversely, at higher water contents, OH radicals concentrate in the core of the discharge with the highest density close to the edge of the quartz capillary as shown in Fig. 8. It has to be noted that the saturated water pressure in the surrounding air at 293 K is about 6×10^{21} m^{-3}. As shown in Fig. 6, about 2% of this water quantity $\sim 1.2 \times 10^{20}$ m^{-3} can come to the plasma due to air back diffusion. This value is of the same order as H$_2$O admixture in the feed gas when OH distribution transfers from the ring shape to the cylindrical. Based on the fact that the OH density just varies only by a factor of three, we can expect that the production mechanism of the OH radicals in the jet core and outer zone at low water content is probably the same. The expected densities of OH$^+$ and excited states of nitrogen N$_2$(A) and N$_2$(^{2}D) are much lower than the density of Ar^m and correspondingly the main pathway of OH production will be through argon metastable-neutral reactions. On the other hand, electron impact dissociation of water starts to be dominant in the OH(X) production at higher water density.[13] Indeed, at the water content varying from 0.15% to 0.3%, the region of OH radicals generation switches from the outer part of the plasma jet to the core of the discharge where electrons density is high. At higher H$_2$O admixing, the OH density slowly decreases to minimum of 10^{18} m^{-3} corresponding to H$_2$O content of 1%. A further increase of water admixture causes the plasma to extinguish. We would like to note that the variation of water content not only allows changing OH production rate but also the place where radicals are generated, see Fig. 8. It could be interesting for the application of the plasma jet in, e.g., medicine or dental care: at low water content >0.15%, OH radicals are produced in spatially broad jet, whereas at water content of 0.3% the generation of radicals is much higher and also

limited by the central part of the jet so focused local treatment can be achieved.

IV. CONCLUSIONS

In the present work, the distribution of OH radicals in RF plasma was studied as a function of water content in gas forming mixture. OH radicals, as one of the most important species in the plasma jet applications, are studied by means of laser-induced fluorescence spectroscopy. It is shown that vibrational and rotational energy transfers after the laser excitation are of primary importance in the LIF diagnostics at atmospheric pressure. Laser excited OH radicals are not thermalized and the rotational distribution after laser excitation does not follow the Boltzmann distribution. Energy transfer processes have been taken into account in the model of OH radicals excitation though the calculation of the fluorescence yield. The model has been used in order to obtain axial and radial 2D maps of the absolute OH densities at different water contents. The effect of H$_2$O addition on the OH radicals generation is investigated and discussed based on the experimental results. The found distribution of radicals is consistent with the geometry of the plasma jet, which indicates that the generation of OH radicals takes place inside the plume region. The highest density of 1.15×10^{20} m^{-3} is measured in closest distance to the plasma core for the case of 0.3% H$_2$O.

[1] E. Stoels, I. E. Kieft, R. E. J. Sladek, L. J. M. van den Bedem, E. P. van der Laan, and M. Steinbuch, Plasma Sources Sci. Technol. **15**, S169 (2006).

[2] J. Benedikt, K. Focke, A. Yanguas-Gil, and A. von Keudell, Appl. Phys. Lett. **89**, 251504 (2006).

[3] X. Lu, Z. Jiang, Q. Xiong, Z. Tang, and Y. Pan, Appl. Phys. Lett. **92**, 151504 (2008).

[4] P. Bruggeman and C. Leys, J. Phys. D: Appl. Phys. **42**, 053001 (2009).

[5] R. Ono, Y. Teramoto, and T. Oda, Plasma Sources Sci. Technol. **19**, 015009 (2010).

[6] A. Sarani, A. Nikiforov, and C. Leys, Phys. Plasmas **17**, 063504 (2010).

[7] V. N. Ochkin, *Spectroscopy of Low Temperature Plasma* (Wiley-VCH, Weinheim, 2009), p. 609.

[8] N. Knake, K. Niemi, S. Reuter, V. S. der Gathen, and J. Winter, Appl. Phys. Lett. **93**(13), 131503 (2008).

[9] A. Nikiforov, Q. Xiong, N. Britun, R. Snyders, X. P. Lu, and C. Leys, Appl. Phys. Express **4**(2), 026102 (2011).

[10] S. Yonemori, Y. Nakagawa, R. Ono, and T. Oda, J. Phys. D: Appl. Phys. **45**, 225202 (2012).

[11] N. Srivastava and C. Wang, J. Appl. Phys. **110**, 053304 (2011).

[12] T. Verreycken, D. C. Schram, C. Leys, and P. Bruggeman, Plasma Sources Sci. Technol. **19**, 045004 (2010).

[13] D. X. Liu, P. Bruggeman, F. Iza, M. Z. Rong, and M. G. Kong, Plasma Source Sci. Technol. **19**, 025018 (2010).

[14] I. A. Soloshenko, V. V. Tsiolko, S. S. Pogulay, A. G. Kalyuzhnaya, V. Yu. Bazhenov, and A. I. Shchedrin, Plasma Sources Sci. Technol. **18**, 045019 (2009).

[15] J. T. Salmon and N. M. Laurendeau, Appl. Opt. **24**, 65 (1985).

[16] L. R. Williams and D. R. Crosle, J. Chem. Phys. **104**(17), 6507 (1996).

[17] J. Luque and D. R. Crosley, LIFBASE: Database and spectral simulation (version 1.5), SRI International Report No. MP 99-009, 1999.

[18] P. H. Paul, J. Quant. Spectrosc. Radiat. Transfer. **51**(3), 511 (1994).

[19] M. T. Berry, M. R. Brustein, and M. I. Lester, J. Chem. Phys. **92**(11), 6469 (1990).

[20] S. Kanazawa, H. Tanaka, A. Kajiwara, T. Ohkubo, Y. Nomoto, M. Kocik, J. Mizeraczyk, and J. Chang, Thin Solid Films **515**, 4266 (2007).

[21] U. Rahmann, A. Bulter, U. Lenhard, R. Dusing, D. Markus, A. Brockhinke, and K. Kohse-Hoinghaus, LASKIN—A Simulation Program for Time-Resolved LIF-Spectra, Internal Report, University of Bielefeld, Faculty of Chemistry, Physical Chemistry I (2003).

[22] I. J. Wysong, J. B. Jeffries, and D. R. Crosley, J. Chem. Phys. **92**(9), 5218 (1990).

[23] R. Kienle, M. P. Lee, and K. Kohse-Hoinghaus, Appl. Phys. B **62**, 583–599 (1996).

[24] O. Eichwald, M. Yousfi, A. Hennad, and M. D. Benabdessadok, J. Appl. Phys. **82**, 4781 (1997).

[25] Y. Itikawa, J. Phys. Chem. Ref. Data **34**, 1 (2005).

[26] NIST Chemical Kinetics Database, Standard Reference Database 17, Version 7.0 (Web Version), Release 1.4.2, Data Version 2009.01 (http://kinetics.nist.gov/kinetics/).

[27] M. Tamura, P. A. Berg, J. E. Harrington, J. Luque, J. B. Jeffries, G. P. Smith, and D. R. Crosley, Combust. Flame **114**, 502–514 (1998).